Biomass Conversion and Biorefinery
https://doi.org/10.1007/s13399-024-05529-x

ORIGINAL ARTICLE

Biosynthesis of zirconia nanoparticles (ZrO_2) by water hyacinth: characterization and its photocatalytic dye degradation activity

Shivam Pandey[1] · Jyoti Chaudhary[1] · Himani Sharma[1] · Shefali Pundir[1] · Sarvesh Rustagi[2] · Sumira Malik[3] · Priyvart Choudhary[4]

Received: 7 July 2023 / Revised: 2 November 2023 / Accepted: 5 November 2023

Abstract
The green biogenic production of nanoparticles from natural sources is always desirable due to its minimal environmental effect. In this study, the generation of ZrO_2 nanoparticles from the aqueous leaf extract of *Eichhornia crassipes* was the major emphasis. It is a notable weed that poses a threat to aquatic life and the environment owing to its proclivity to cover the whole water surface and is a major environmental hazard. Synthesized ZrO_2 nanoparticles were characterized by using UV–visible, Fourier Transform Infrared Spectroscopy (FTIR), X-Ray Diffraction (XRD), and Scanning Electron Microscopy (SEM). Characterization methods validated the creation of ZrO_2 nanoparticles. Narrow peaks with sharp edges indicated a considerable rise in the zirconia nanoparticle's crystalline index when XRD analysis was done on them. The nanoparticles were then utilized for treating wastewater containing industrial dyes, i.e., Methyl Orange and Methylene Blue. The results indicated maximum removal of COD, BOD, nitrate, and phosphate along with highest degradation of these industrial dyes. The removal efficiency of 72.63% COD, 73.06% of BOD, 84.64% nitrate, and 90.30% phosphate was obtained in wastewater. Moreover, the highest degradation of Methylene Blue and Methylene Orange was found at 40 ppm concentration using 0.02% of ZrO_2 nanoparticles. This study shows that biogenically produced nanoparticles were found to possess a great degrading capacity for treatment of Methyl Orange and Methylene Blue.

Keywords Nanoparticles · Zirconia nanoparticles · Water hyacinth · Aquatic weed · Wastewater treatment · Water pollutants

1 Introduction

The manufacture of textiles demands a substantial amount of water and energy. After dyeing and finalizing their products, factories produce a substantial quantity of polluted water [1]. This water is exceedingly hazardous to humans due to its vast quantity and composition. There are a variety of environmental hazards related with the direct discharge of dyeing wastewater [2]. Wastewater can inflict severe harm to aquatic life, soil, and potable water. In addition, certain dyes and their waste products have the potential to be carcinogenic and toxic. Thus, the dyes must be extracted before disposal. Biodegradation and ultrafiltration, as well as photocatalytic degradation, oxygenation, and adhesion, are among the wastewater treatment approaches that have been investigated. When it comes to treating these effluents containing dyes, conventional adsorption is a very cost-effective and low-cost technology [3].

Nanoparticles are nanotechnology's droplets with distinct physical and chemical characteristics. Nanoparticles are large-category substances composed of at least one dimension less than 100 nm. When scientists recognized that the morphology influences the physicochemical characteristics of these chemicals, they realized the value of these substances [4]. Nanomaterials are used in microbiology, mechanics, the medical sector, a variety of health care facilities, engineering domains, electronics, biotechnology,

✉ Priyvart Choudhary
piryvartpanwar0@gmail.com

1 Department of Chemistry, School of Applied and Life Sciences, Uttaranchal University, Dehradun, India

2 Department of Food Technology, School of Applied and Life Sciences, Uttaranchal University, Dehradun, India

3 Department of Biotechnology, Amity University, Ranchi, Jharkhand, India

4 Department of Biotechnology, School of Applied and Life Sciences, Uttaranchal University, Dehradun, India

Published online: 26 March 2024

and science-related fields due to their most useful attribute, a large specific surface area [5, 6]. Typically, the nanoparticles are composed of three layers: the surface layer, the shell layer, and the nanoparticle core. Due to their extraordinary features, nanoparticles have attracted the attention of several scientific fields. There are several traditional methods available, including physical and chemical procedures, for the manufacture of nanometer-sized particles; however, green synthesis of these particles has piqued the interest of many since it lowers the use of carcinogenic and expensive chemicals. Because plant extract may be utilized in place of toxic chemicals in this process, it is considered an eco-friendly low-cost alternative [7].

Water hyacinth, also known as *Eichhornia crassipes*, is a free-floating aquatic weed native to South America. It has been regarded as invasive across Africa and Asia since the 1990s [8]. The ideal conditions for water hyacinth growth are waters that are rich in nitrogen, phosphorus, and potassium and that are between 28 and 30 °C in temperature. The water hyacinth grows at a very rapid rate in freshwater under ideal circumstances [9]. Water hyacinth may blanket lakes and wetlands, outcompete native aquatic species, lower fish oxygen levels, create the ideal mosquito habitat, control weeds, provide feed, produce biofuel, and purify water. Aquatic invasive species put socioeconomic and ecological systems in peril by encroaching on freshwater environments. Almost all aquatic systems across the world have been invaded by it. The environment and human health suffer because of the water hyacinth's tremendous growth under ideal conditions. *E. crassipes* absorbs lead and cadmium and is extremely tolerant. It is ideal for biocleaning environmental trash. It ferments quickly and produces methane biomass due to its highwater index [10]. Invasive water hyacinth possesses antibacterial, antimicrobial, antiinflammatory, and antioxidant properties that might be valuable in medicine and pharmaceuticals [11]. Water hyacinth has also been used to remove chemicals, dissolved solids, biochemical oxygen demand, suspended particles, total solids, heavy metals, turbidity, and nutrients from wastewater [12–14].

There has been a lot of study on degradation of dyes by using chemical as well as green synthesized metal oxide nanomaterials. Mannaa et al. [15] synthesized TiO_2 and NiO nanoparticles for degrading brilliant green (BG) while Hakam et al. [16] formed silica/bismuth composite for degrading 100% Methylene Blue and brilliant green in 180 min. Saleh et al. [17] also used nickel ferrites for rhodamine dye that reached 99.7% in 90 min. Tayseer et al. [18] used metal oxides of TiO_2 for eliminating MG and Phenol within 45 to 60 min. Due to the environmental harm of synthetic chemicals and the growing interest in earth-friendly nanoparticles, non-harmful, clean, green, and environmentally friendly synthesis is needed [19]. Plant extract reduces and stables nanoparticles, which may aid microbial synthesis because cell culture does not need to be produced, maintained, or restored [20]. Pandey et al. [21] utilized green stannous oxide nanoparticles to remove nitrophenol and dyes. Chemical synthesis without waste detoxification uses gentle pH, pressure, temperature, and environmentally friendly procedures [22]. Recent ZrO_2-NPs were synthesized from *Lycopersicon esculentum* [23], *Helianthus annuus* seed [24], *Curcuma longa* tuber extract [25], etc. extracts.

As per the literature survey, there are a very few researches that have been found on the synthesis of zirconia-derived nanoparticles by using aquatic weeds. Zirconia nanoparticles were prepared by using methanolic extract of leaves of water hyacinth and were further utilized to treat organic dyes. The resultant catalysts were characterized by employing a variety of instruments. The photocatalytic activities of the generated catalysts were investigated by studying their ability to degrade Methylene Blue and Methyl Orange when exposed to visible light. The reusability of the most effective catalyst was meticulously investigated.

2 Materials and method

2.1 Chemical reagents

The chemicals Methylene Blue (MB), Methyl Orange (MO), and zirconia dioxide were purchased from Sigma Aldrich. All the other solvents, glassware, and apparatus were taken from the Department of Chemistry at Uttaranchal University, Dehradun, India. Water hyacinth plant samples were gathered from the Assan Barrage near Dakpathar on the Uttarakhand-Himachal border in India (30°26′09″N, 77°39′09″E), as shown in Fig. 1. Deionized water was further utilized for all the research work.

Fig. 1 Water hyacinth plant

2.2 Synthesis of ZrO_2 nanoparticles

The samples (leaves) were carefully cleaned and dried before being chopped into little pieces. The leaves were subjected to extraction with methanol using the Soxhlet apparatus, followed by evaporation on a hot plate for a duration of 10 to 15 min. In the biological generation of ZrO_2 NPs, a 0.1 M aqueous zirconium dioxide solution was utilized, with a volume of 50 mL, within a 250-mL beaker. A 10 mL solution of *Eichhornia crassipes* leaf extract was introduced to the mixture and subjected to agitation at a temperature of 80 °C for a duration of 2–3 h, followed by a period of undisturbed rest. The ZrO_2 nanoparticles were subsequently transferred to a Petri dish and subjected to a heating process at a temperature of 50 °C for a duration of 10–15 min. Subsequently, the particles were subjected to a thermal treatment in a furnace for approximately 3 h at a temperature of 700 °C, resulting in the production of metal oxide nanoparticles. The stepwise process for nanoparticle synthesis is shown in Fig. 2.

2.3 Characterization of formed particles

The samples were characterized by several different analytical techniques. The crystal structure of the sample was determined by using Rigaku, Smart Lab-XRD. For UV–Vis spectroscopy, Labman-LMSP-UV1900 was used while for morphological study by SEM, Zeiss EVO18 was utilized. The FTIR was done by Thermo Scientific, Summit Lite.

2.4 Photocatalytic activity

In this study, ZrO_2 nanoparticles were synthesized and employed for the degradation of Methyl Orange (MO) and Methylene Blue (MB) dyes under solar light irradiation. After a period of 30 min, the process of dark agitation successfully reached a state of desorption-adsorption equilibrium. Subsequently, the experiment was subjected to sun irradiation, and alterations in the absorbance maxima were observed by employing a double-beam spectrophotometer at predetermined time intervals.

The percentage (%) degradation rate constant was calculated by using the equation given below, where C_i is the initial concentration and C_f is the final concentration.

$$Percentdegradation(\%degradation) = \frac{C_f - C_i}{C_i} \times 100$$

The light source excites the electrons from the valence band (VB) to the conduction band (CB), resulting in the creation of a positive hole within the VB. These charges subsequently facilitate the processes of oxidation and reduction. The process involves the reaction of dissolved oxygen with

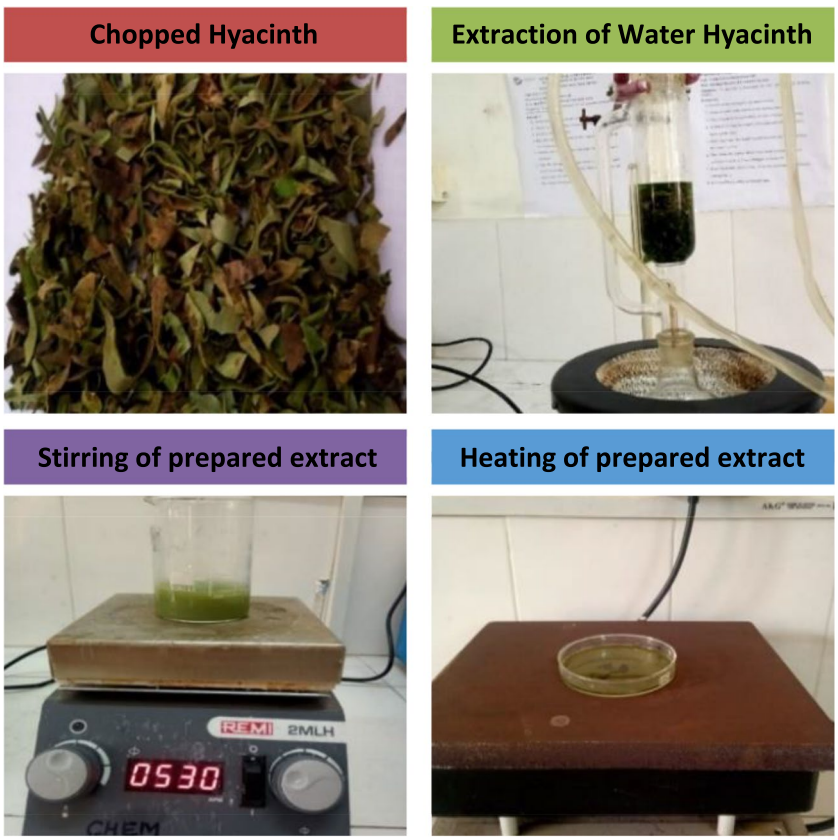

Fig. 2 Preparation of leaf extract for zirconia nanoparticle synthesis

excited electrons, resulting in the formation of superoxide radicals. These radicals subsequently react with hydrogen ions, leading to the production of hydrogen peroxide and hydroxyl radicals. The positive hole undergoes a reaction with surface hydroxyl groups or water molecules, resulting in the formation of hydroxyl radicals. The hydroxyl radicals facilitate the mineralization process of Methyl Orange (MO) and Methylene Blue (MB), resulting in the conversion of these compounds into carbon dioxide (CO_2) and water (H_2O) [26–28].

The mechanism of photocatalysis can be given as follows:

$$ZrO_2 + h\nu \rightarrow e^- + h^+$$

$$O_2 + e^- \rightarrow O_2$$

$$h + OH^- \rightarrow OH\bullet$$

$$h + H_2O \rightarrow H^+ + OH\bullet$$

$$O^{2-}\bullet + \text{MethyleneBlue/MethylOrange} \rightarrow \text{Degradationproducts}$$

$$OH\bullet^- + \text{MethyleneBlue/MethylOrange} \rightarrow \text{Degradationproducts}$$

3 Result and discussions

The presence of ZrO_2 NPs was confirmed by the development of a milky white precipitate. The transformation of zirconia dioxide into nanosized ZrO_2 colloidal particles was indicated by the white colloidal suspension. The absorbance peaks at 300 nm confirmed the presence of ZrO_2 NPs. The interaction of Zr ions with water molecules resulted in the formation of ZrO_2, which then reacted with the aqueous solution to generate nanoparticles. The FTIR spectrum was examined to determine the functional groups of the produced nanoparticles as shown in Fig. 3(a). The existence of the material, the process used for manufacture, the structure of the nanoparticles in solid form, and other factors all influenced the FTIR spectrum of ZrO_2. 1404.845 cm^{-1}, 1610.421 cm^{-1}, 2006.242 cm^{-1}, 2925.093 cm^{-1}, 3460.363 cm^{-1}, and 3543.401 cm^{-1} are the peaks of ZrO_2. The FTIR spectrum confirmed the formation of the ZrO_2 structure. For ZrO_2, significant absorption band is found in the region from 3200 to 3800 cm^{-1} owing to the stretching vibration – OH group of water molecule adsorbed on ZrO_2 nanoparticles and peak centered at 2006.24 cm^{-1} relates to distinctive bending vibration. The peaks at 2925.09 cm^{-1} suggest hydroxyl zirconia (Zr–OH) bond stretching. Sharp peaks at 500 cm^{-1} indicate that ZrO_2 is crystalline [29–31]. The extract contains flavonoids, phenolic, and other

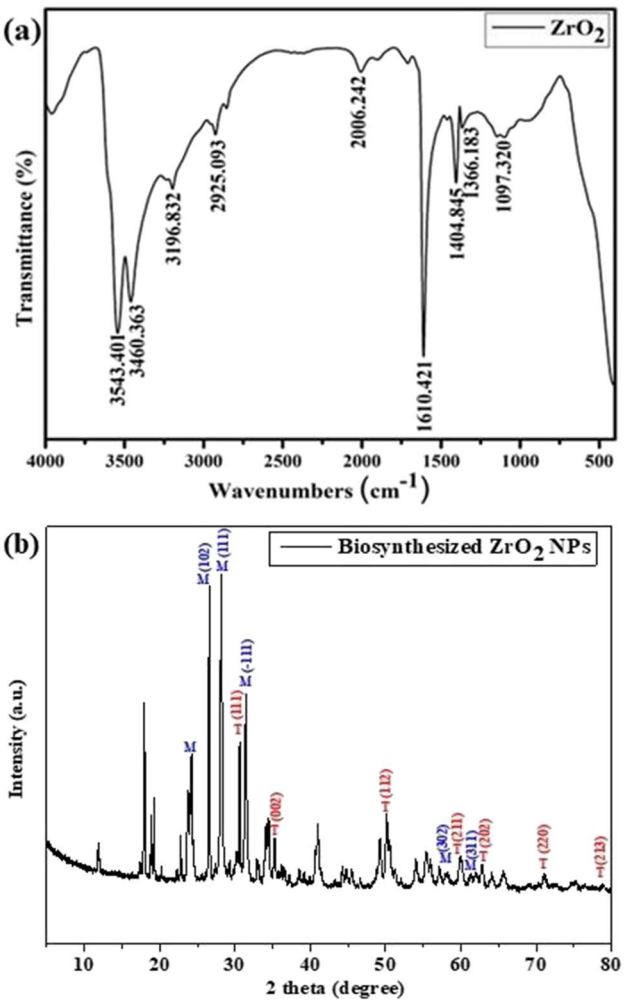

Fig. 3 FTIR analysis (**a**) and XRD pattern (**b**) of zirconia nanoparticles

phytochemical substances that reduce and stabilize zirconia slats, controlling green synthesis size. The FT-IR spectra also suggest a mechanism for biosynthesizing ZrO_2-NPs from extract. Briefly, phytochemicals in leaf extract initially convert Zr^{2+} ions to zero-valent Zr atoms. Zero-valent Zr atoms commence nucleation, reduce leftover Zr^{2+} to ZrO, and expand to form clusters.

To confirm the phases and the purity of biosynthesized ZrO_2 NPs, the XRD pattern was recorded. Figure 3(b) shows the monoclinic (M) and tetragonal (T) phases of NPs present in the as-prepared sample. The monoclinic and tetragonal phases of ZrO_2 NPs can be determined by using the intensities of their equivalent peaks of XRD spectra. The diffraction patterns of ZrO_2 NPs at 2θ and lattice planes (*hkl*) of 30.48° (101), 35.16° (110), 50.64° (112), 60.26° (211), 63.14° (202), 74.63° (220), and 81.67° (213), respectively [32, 33], confirm the tetragonal phase of ZrO_2 crystalline system and perfectly matched with the JCPDS Card No. 81–1455 and

a more intense characteristic peak at $2\theta = 30.48°$ associated to (101) lattice plane while the peaks at 28.2° (111), 31.36° (− 111), 60.10° (302), and 62.89 (311), respectively, confirm the good arrangement with monoclinic phase (JCPDS Card No. 83–0944) [34, 35]. The crystallite size of monoclinic and tetragonal ZrO_2 NPs was calculated by using the Debye-Scherer equation formula $D = K\lambda/\beta\cos\theta$, where k is equal to 0.9 and refers to the shape factor or correction factor, β is the full width at half maximum (FWHM) of the diffraction peak at angle 2θ and plane (hkl), λ is the Cu-Kα, $\lambda = 1.5406$ Å an X-ray wavelength, θ (in degree) is the Bragg diffraction angle, and D is the crystallite size. We have measured the crystalline size for the highly intense peaks at (101) and (− 111) crystal planes of tetragonal and monoclinic ZrO_2 structure. The predictable value of average crystal size of biosynthesized ZrO_2 NPs is found to be around 13.12 nm. Moreover, monoclinic and tetragonal structures are well-defined with monoclinic and tetragonal unit cells with the symmetry defined via the space groups P21/c and P42/nmc, respectively. It is well defined that smaller the crystallite size shows the presence of O_2 vacancies at grain boundaries and at the surface, which result in the prevention of the growth of nanoparticles and generate a field stress [36]. Field stress produces the crystal defects that act as a scattering center for electron (e^-) and hole (h^+) as well as the excitation of the recombination of e^--h^+ pairs which affect the photocatalytic performance [37].

Figure 4 demonstrates the SEM analysis of ZrO_2 NPs which revealed the importance of ZrO_2 in maintaining the nanostructure phase. The zirconia nanoparticles were found to be agglomerated.

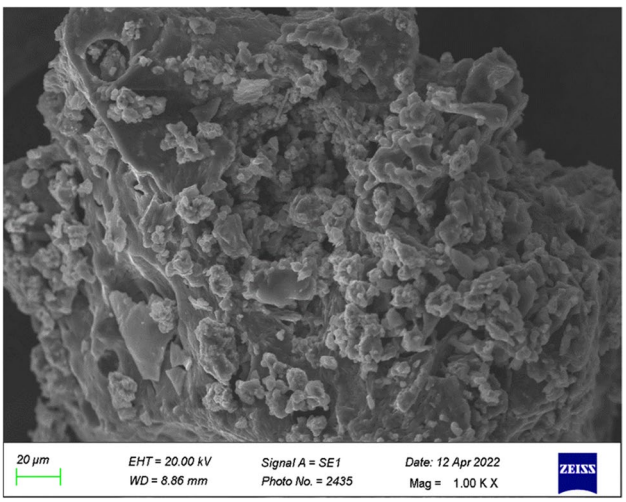

Fig. 4 SEM image of zirconia nanoparticles

4 Degradation activity of Methyl Orange and Methylene Blue

4.1 Impact of varying concentration of catalyst dose

Under sunlight, the photodegradation of MO and MB is done through varying doses of ZrO_2 NPs. Figure 5(a)(b) show that as the amount of catalyst was increased, the percentage of degradation of dyes went up, and the most degradation was seen when 0.2 g/L of catalyst dose was used. The pH of both solutions used in the experiment was kept at 7 before the experiment began, but it was not kept that way after that. The drop in the degradation percentage of Methyl Orange and Methylene Blue that are broken down can be explained by the fact that a larger dose of catalyst starts blocking the light, which also slows down the photocatalytic activity. The most Methyl Orange solution could break down was 98.73%, and the most Methylene Blue solution could break down was 99.96%.

4.2 Impact of varying concentration of dye

The photocatalytic activity of ZrO_2 NPs was evaluated by applying 0.2 g/L of catalyst (optimum dose) at different concentrations of 20, 40, 60, 80, and 100 ppm of MO and MB solutions. Dye concentration was found to significantly affect photocatalytic activity as well. Figure 6(a),(b) show the graphs for varying concentration of MO and MB dyes. The graph depicts a gradual decline in photocatalytic activity following a rise in activity up to 40 ppm, because of further increases in concentration. At 40 ppm, the most noticeable photocatalytic activity was observed. Due to maximum penetration of light, there is initially greater interaction between the light and the photocatalyst, but as the dye concentration increases, the dye molecules start blocking the penetrating light, thus reducing the photocatalyst's effectiveness.

4.3 Impact of varying pH

As shown in Fig. 7(a),(b), the photocatalytic activity was also evaluated by increasing the pH from 3 to 11 while holding all other reaction conditions constant. With increase in pH, the response rate increased, but further increase slowed the rate of deterioration. To investigate the effect of pH, 0.2 g/L ZrO_2 NPs were put to a 40 ppm MO and MB solution, and the highest degradation was observed at pH 9, indicating that alkaline media promotes degradation more effectively than acidic media. In the presence of sunlight, when organic chemicals interact with dissolved oxygen, they dissociate and cause photooxidation. As the pH of a

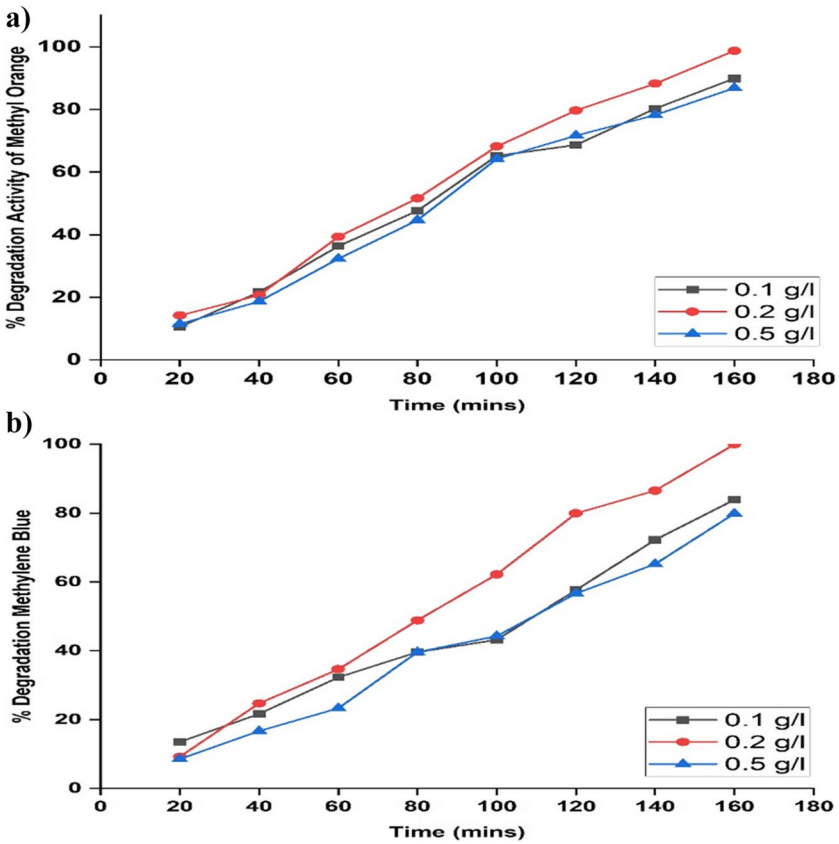

Fig. 5 Effect of different catalytic dose on degradation of MO (**a**) and MB (**b**) at 160 min and 10 ppm concentration

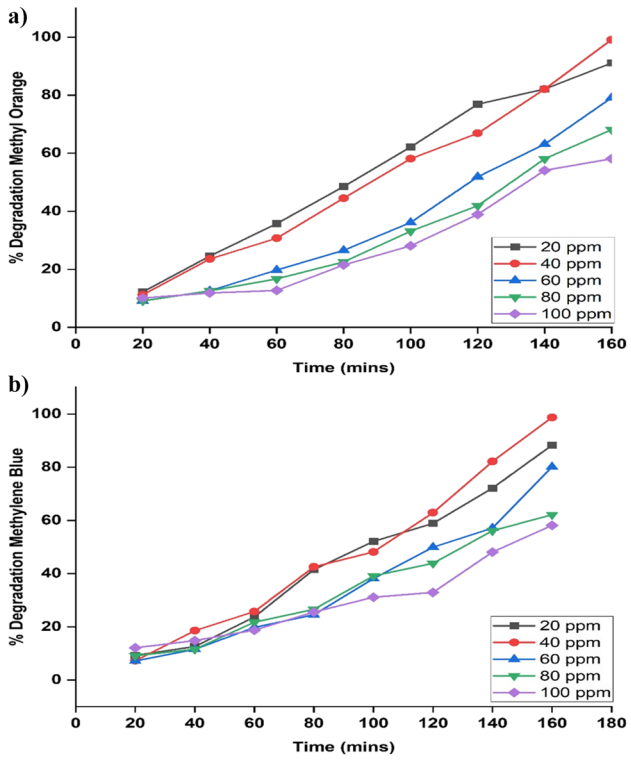

Fig. 6 Effect of different concentration of MO (**a**) and MB dye (**b**) at 160 min and 0.2-g/L dose

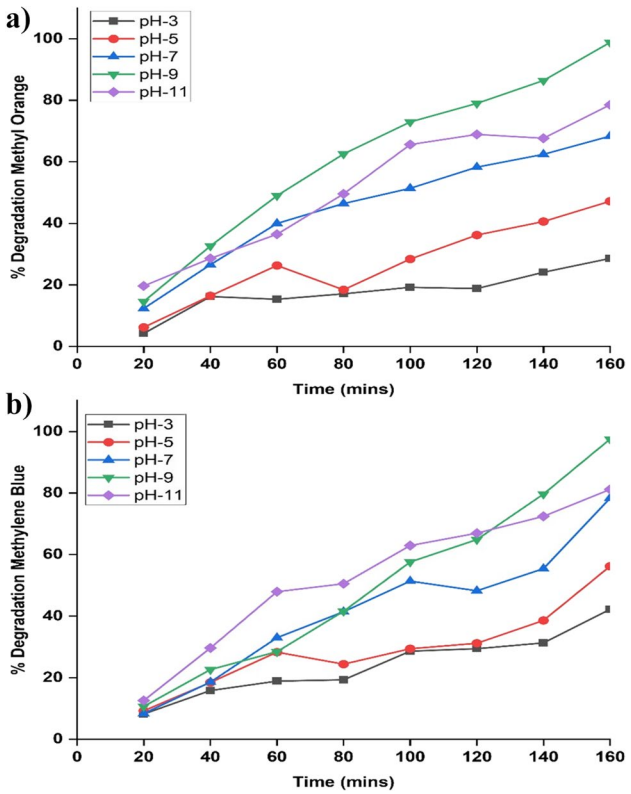

Fig. 7 Effect of pH variation on degradation of **a** MO and **b** MB at 160 min and 40 ppm concentration

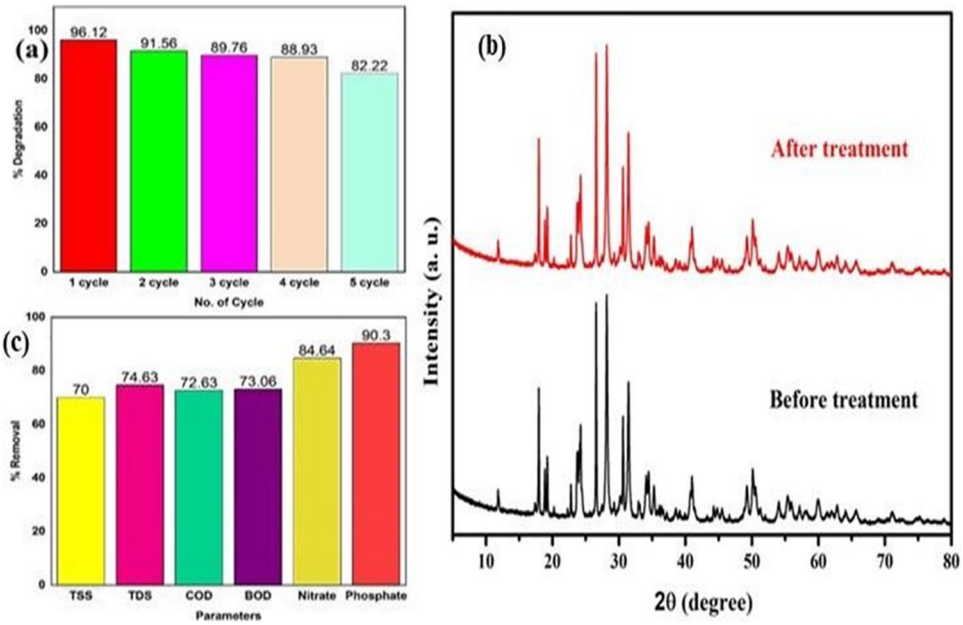

Fig. 8 **a** Reusability of ZrO_2 NPs, **b** XRD pattern of ZrO_2 NPs before and after the degradation of MB and MO, and **c** % removal efficiency of different parameters using ZrO_2 NPs

particle's surface alters, a dispersed state develops. Moreover, Van Der Waals forces prevent the agglomeration and promote dispersion because ZrO_2 nanoparticles lack charge.

4.4 Antibacterial activity

The disk diffusion method was used to test the NPs for *Staphylococcus aureus* (gram-positive) and *Escherichia coli* (gram-negative). *S. aureus* was found to be more sensitive to green-assisted ZrO_2 NPs than *E. coli*. *S. aureus* and *E. coli* growth is controlled by Zr^{4+} ions which cause cell wall membrane breaches. The plant extract combination with ZrO_2 NPs boosted radical generation and ROS (reactive oxygen species). The accepted metal ions in the bacterial framework electrostatically produce ZrO_2 NPs via ROS.

4.5 Reusability

In addition, the photocatalytic stability of ZrO_2 NPs was assessed after five cycles under the same reaction conditions and with the addition of just fresh dye solutions. The percentage of decomposition was recorded for each of the five cycles, decreasing from cycle 1 to cycle 5. Before being reused, the catalyst was separated by centrifugation and then cleaned with ethanol and distilled water each time it was recycled. The catalyst displayed substantial activity and could be reused up to 5 times consecutively without appreciable activity loss. This decline may be attributable to the saturation of the catalyst's surface, where numerous molecules are adsorbed and prevent light from reaching the nanoparticles' surface, thereby reducing the electron excitation process and, consequently, the production of hydroxyl radicals and reactive oxygen species. The number displayed in Fig. 8(a) is the mean value obtained from the reusability test using both Methyl Orange and Methylene Blue dyes. Figure 8(b) shows the stability test analysis of reused photocatalysts by using the XRD analysis to know the morphological robustness, chemical compositional, and oxidation state changes of photocatalysis during the treatment. It is observed that no impurity peaks were formed in the XRD pattern of reused catalyst which shows that no photo corrosion and leaching of the catalyst generated during the dye removal. In general, after treatment as-prepared photocatalysts still preserve almost its crystallinity and superb stability under the treatment condition [38].

4.6 Treatment of wastewater using zirconia nanoparticles

The wastewater collected from the Tons River in Dehradun was treated using the created nanoparticles. Throughout the operation, there was a shift in the pH of the effluent. The samples were analyzed with the standard procedures developed by the APHA in 1995. The results of these analyses were noted and tabulated in Table 1. Figure 8(c) demonstrates the reusability, XRD pattern, and removal efficiency of ZrO_2 NPs in wastewater.

5 Conclusion

In a nutshell, zirconia oxide nanoparticles were synthesized by using an aquatic weed. It was applied to determine the removal efficiency of various pollutants from the wastewater,

Table 1 % Removal efficiency of different parameters using ZrO_2 NPs in wastewater

Parameters	Initial values (mg/L)	Value after addition of ZrO_2 NPs (mg/L)	Percentage removal efficiency (%)
Total suspended solids (TSS)	120	36	70
Total dissolved solids (TDS)	615	156	74.63
Chemical oxygen demand (COD)	542	148	72.63
Biochemical oxygen demand (BOD)	349	94	73.06
Nitrate	28	4.3	84.64
Phosphate	33	3.2	90.3

like nitrate, phosphate, COD, BOD, TSS, and TDS. The synthesized nanoparticles had found an exceptionally high clearance percentage for these contaminants along with very good degradation activity of Methyl Orange and Methylene Blue. In addition, it was found that a dosage of 20 mg of nanoparticles, when added to a 40 ppm solution of Methyl Orange and Methylene Blue at pH 9, demonstrated the highest degree of degradation. During 2.5 h, it was observed that 99% of Methyl Orange and Methylene Blue was degraded using 20 mg (0.02%) of nanoparticles. This study demonstrates the synthesis and applications of zirconia nanoparticles using aquatic plants, which could be considered a successful application of the "Best out of trash" concept, and it will pave the way for additional research to be conducted in large scale.

Author contribution S. P. and P. C. conceptualized the study and designed the methodology. S. P., J. C., H. S., and S. P. conducted the experimental studies. S. P., R. S., P. C., and S. R. conducted the literature survey and interpretation of results. S. P., R. S., and P. C. prepared the initial and revised draft of the manuscript.

Data availability Data available on request.

Declarations

Ethical approval Authors declared no ethical issue in present study.

Competing interests The authors declare no competing interests.

References

1. Aboelfetoh EF, Gemeay AH, El-Sharkawy RG (2020) Effective disposal of methylene blue using green immobilized silver nanoparticles on graphene oxide and reduced graphene oxide sheets through one-pot synthesis. Environ Monit Assess 192:1–20
2. Hussain MK, Khalid NR (2022) Surfactant-assisted synthesis of MoO_3 nanorods and its application in photocatalytic degradation of different dyes in aqueous environment. J Mol Liq 346:117871
3. Wenjie Z, Zhou C, Zhou W, Lei A, Zhang Q, Wan Q, Zou B (2011) Fast and considerable adsorption of methylene blue dye onto graphene oxide. Bull Environ Contam Toxicol 87:86–90
4. Pandit C, Roy A, Ghotekar S, Khusro A, Islam MN, Emran TB, Lam SE, Khandaker MU, Bradley DA (2022) Biological agents for synthesis of nanoparticles and their applications. J King Saud Univ Sci 34(3):101869
5. Mandal AK, Katuwal S, Tettey F, Gupta A, Bhattarai S, Jaisi S, Bhandari DP, Shah AK, Bhattarai N, Parajuli N (2022) Current research on zinc oxide nanoparticles: synthesis, characterization, and biomedical applications. Nanomaterials 12(17):3066
6. Ahmad W, Joshi HC, Pandey S, Kumar V, Verma M (2022) An overview of green methods for Fe_2O_3 nanoparticle synthesis and their applications. Int Nano Lett 3:1–4
7. Jeevanandam J, Kiew SF, Boakye-Ansah S, Lau SY, Barhoum A, Danquah MK, Rodrigues J (2022) Green approaches for the synthesis of metal and metal oxide nanoparticles using microbial and plant extracts. Nanoscale 14(7):2534–2571
8. Dersseh MG, Melesse AM, Tilahun SA, Abate M, Dagnew DC (2019) Water hyacinth: review of its impacts on hydrology and ecosystem services—lessons for management of Lake Tana. Extreme hydrology and climate variability. 1:237-51
9. Lima JR, De Farias DL, Menezes TH, Oliveira RV, Silva IA, da Costa CG, Romão LP (2020) Potential of a magnetic hybrid material produced using water hyacinth (Eichhornia crassipes) for removal of inorganic and organic pollutants from aqueous media. J Environ Chem Eng 8(5):104100
10. Lalitha P, Sripathi SK, Jayanthi P (2012) Secondary metabolites of Eichhornia crassipes (water hyacinth): a review (1949 to 2011). Nat Prod Commun 7(9):1934578X1200700939
11. Das S, Goswami S, Talukdar AD (2016) Physiological responses of water hyacinth, Eichhornia crassipes (Mart.) Solms, to cadmium and its phytoremediation potential. Turk J Biol 40(1):84–94
12. Auchterlonie J, Eden CL, Sheridan C (2021) The phytoremediation potential of water hyacinth: a case study from Hartbeespoort Dam, South Africa. S Afr J Chem Eng 37:31–36
13. Rezania S, Ponraj M, Talaiekhozani A, Mohamad SE, Din MF, Taib SM, Sabbagh F, Sairan FM (2015) Perspectives of phytoremediation using water hyacinth for removal of heavy metals, organic and inorganic pollutants in wastewater. J Environ Manage 163:125–133
14. Joseph L, Jun BM, Flora JR, Park CM, Yoon Y (2019) Removal of heavy metals from water sources in the developing world using low-cost materials: a review. Chemosphere 229:142–159
15. Mannaa MA, Qasim KF, Alshorifi FT, El-Bahy SM, Salama RS (2021) Role of NiO nanoparticles in enhancing structure properties of TiO_2 and its applications in photodegradation and hydrogen evolution. ACS Omega 6(45):30386–30400
16. El-Hakam SA, ALShorifi FT, Salama RS, Gamal S, El-Yazeed WA, Ibrahim AA, Ahmed AI (2022) Application of nanostructured mesoporous silica/bismuth vanadate composite catalysts for the degradation of methylene blue and brilliant green. J Mater Res Technol 18:1963–1976

17. Saleh TS, Badawi AK, Salama RS, Mostafa MMM (2023) Design and development of novel composites containing nickel ferrites supported on activated carbon derived from agricultural wastes and its application in water remediation. Materials 16(6):2170
18. Alasri, T. M., Ali, S. L., Salama, R. S., & Alshorifi, F. T. (2023). Band-structure engineering of TiO_2 photocatalyst by AuSe quantum dots for efficient degradation of malachite green and phenol. J Inorg Organomet Polym Mater, 1–12
19. Vinu D, Govindaraju K, Vasantharaja R, Amreen Nisa S, Kannan M, Vijai Anand K (2021) Biogenic zinc oxide, copper oxide and selenium nanoparticles: preparation, characterization and their anti-bacterial activity against Vibrio parahaemolyticus. J Nanostruct Chem 11:271–286
20. Omidi S, Sedaghat S, Tahvildari K, Derakhshi P, Motiee F (2018) Biosynthesis of silver nanocomposite with Tarragon leaf extract and assessment of antibacterial activity. J Nanostruct Chem 8:171–178
21. Pandey, S., Singh, A., Ahmad, W., Panwar, R., & Anand, S. (2023). Aquatic weed derived SnO_2 nanoparticle: synthesis, characterization and its application for degradation of dyes and wastewater treatment. Asian J Chem
22. Muthuvel A, Jothibas M, Manoharan C (2020) Synthesis of copper oxide nanoparticles by chemical and biogenic methods: photocatalytic degradation and in vitro antioxidant activity. Nanotechnol Environ Eng 5:1–19
23. Shinde HM, Bhosale TT, Gavade NL, Babar SB, Kamble RJ, Shirke BS, Garadkar KM (2018) Biosynthesis of ZrO_2 nanoparticles from Ficus benghalensis leaf extract for photocatalytic activity. J Mater Sci: Mater Electron 29:14055–14064
24. Muthulakshmi N, Kathirvel A, Subramanian R, Senthil M (2023) Biofabrication of zirconia nanoparticles: synthesis spectral characterization and biological activity evaluation against pathogenic bacteria. Biointerface Res Appl Chem 13:190
25. Saraswathi VS, Santhakumar K (2017) Photocatalytic activity against azo dye and cytotoxicity on MCF-7 cell lines of zirconium oxide nanoparticle mediated using leaves of Lagerstroemia speciosa. J Photochem Photobiol, B 169:47–55
26. Horti NC, Kamatagi MD, Nataraj SK, Wari MN, Inamdar SR (2020) Structural and optical properties of zirconium oxide (ZrO_2) nanoparticles: effect of calcination temperature. Nano Express 1(1):010022
27. Kumar S, Bhunia S, Ojha AK (2015) Effect of calcination temperature on phase transformation, structural and optical properties of sol-gel derived ZrO_2 nanostructures. Physica E 66:74–80
28. Turki Jalil A, Emad Al Qurabiy H, Hussain Dilfy S, Oudah Meza S, Aravindhan SM, Kadhim MM, Aljeboree A (2021) CuO/ZrO2 nanocomposites: facile synthesis, characterization and photocatalytic degradation of tetracycline antibiotic. J Nanostruct 11(2):333–346. https://doi.org/10.22052/JNS.2021.02.014
29. Sikdar S, Banu A, Ali S, Barman S, Kalar PL, Das R (2022) Micro-structural analysis and photocatalytic properties of green synthesized t-ZrO_2 nanoparticles. Chemistry 7(4):202103953
30. Haq S, Shoukat S, Rehman W, Waseem M, Shah A (2020) Green fabrication and physicochemical investigations of zinc-cobalt oxide nanocomposite for wastewater treatment. J Mol Liq 318:114260
31. Choudhary P, Sharma R, Kumar V et al (2023) Synthesis, characterization and catalytic activity of bio-MCM-41 for production of bio crude oil via pyrolysis of rice straw. Waste Biomass Valor. https://doi.org/10.1007/s12649-023-02124-5
32. Horti NC, Kamatagi MD, Nataraj SK, Wari MN, Inamda SR (2020) Structural and optical properties of zirconium oxide (ZrO_2) nanoparticles: effect of calcination temperature. Nano Express 1:010022
33. Ibrahim AA, Salama RS, El-Hakam SA, Khder AS, Ahmed AI (2021) Synthesis of sulfated zirconium supported MCM-41 composite with high-rate adsorption of methylene blue and excellent heterogeneous catalyst. Colloids Surf, A 616:126361
34. Zhang R, Liu H, He D (2012) Pure monoclinic ZrO_2 prepared by hydrothermal method for isosynthesis. Catal Commun 26:244–247
35. Shah A, Haq S, Rehman W, Waseem M, Shoukat S, Rehman MU (2019) Photocatalytic and antibacterial activities of Paeonia emodi mediated silver oxide nanoparticles. Materials Research Express 6(4):045045
36. Singh S, Srivastava VC, Singh A, Kumar P, Lo SL (2023) Synthesis, characterization, and catalytic application of CuO for perfluorooctanoic acid decomposition with PMS activation. Materi Today Commun 34:105–107
37. Singh S, Rawat S, Patidar R, Lo SL (2022) Photocatalystic degradation of bisphenol A with bismuth-based multi-metal oxide: kinetics of process optimization and degradation mechanism. Water Sci Technol 86(12):32483263
38. Singh S, Srivastava VC, Lo SL, Mandal TK, Naresh G (2017) Morphology-controlled green approach for synthesizing the hierarchical self-assembled 3D porous ZnO superstructure with excellent catalytic activity. Microporous Mesoporous Mater 239:296–309